5968–5979 *Nucleic Acids Research, 2017, Vol. 45, No. 10* *Published online 27 April 2017*
doi: 10.1093/nar/gkx294

The dynamics of the monomeric restriction endonuclease BcnI during its interaction with DNA

Georgij Kostiuk[1,†], Jasmina Dikić[2,†], Friedrich W. Schwarz[3], Giedrius Sasnauskas[1], Ralf Seidel[2,*] and Virginijus Siksnys[1,*]

[1]Institute of Biotechnology, Vilnius University, Sauletekio av. 7, LT-10257 Vilnius, Lithuania, [2]Molecular Biophysics group, Institute for Experimental Physics I, Universität Leipzig, Linnéstr. 5, 04103 Leipzig, Germany and [3]BCUBE, Technische Universitaet Dresden, Arnoldstrasse 18, 01307 Dresden, Germany

Received December 29, 2016; Revised April 07, 2017; Editorial Decision April 10, 2017; Accepted April 13, 2017

ABSTRACT

Endonucleases that generate DNA double strand breaks often employ two independent subunits such that the active site from each subunit cuts either DNA strand. Restriction enzyme BcnI is a remarkable exception. It binds to the 5′-CC/SGG-3′ (where S = C or G, '/' designates the cleavage position) target as a monomer forming an asymmetric complex, where a single catalytic center approaches the scissile phosphodiester bond in one of DNA strands. Bulk kinetic measurements have previously shown that the same BcnI molecule cuts both DNA strands at the target site without dissociation from the DNA. Here, we analyse the BcnI DNA binding and target recognition steps at the single molecule level. We find, using FRET, that BcnI adopts either 'open' or 'closed' conformation in solution. Next, we directly demonstrate that BcnI slides over long distances on DNA using 1D diffusion and show that sliding is accompanied by occasional jumping events, where the enzyme leaves the DNA and rebinds immediately at a distant site. Furthermore, we quantify the dynamics of the BcnI interactions with cognate and non-cognate DNA, and determine the preferred binding orientation of BcnI to the target site. These results provide new insights into the intricate dynamics of BcnI–DNA interactions.

INTRODUCTION

Many vital cellular processes, including DNA replication, transcription, DNA repair, gene expression control, recombination and antiviral defense are mediated by proteins and enzymes that recognize specific DNA targets. Type II restriction endonucleases (REases) form one of the largest groups of site-specific DNA-acting enzymes that recognize short DNA sequences and cleave both DNA strands within or close to the recognition site. REases are part of restriction-modification systems that provide a defense barrier against invading bacteriophages. Currently, over 4000 enzymes specific for more than 300 different DNA sequence motifs are listed in REBASE (1). Orthodox Type II REases are homodimers that use two separate active sites located in different subunits to cut individual DNA strands in palindromic 4–8 bp DNA sequences. This strategy, however, cannot be generalized for all REases. For example, BcnI restriction enzyme recognizes a pseudopalindromic DNA sequence 5′-CC/SGG-3′ (where S stands for C or G, '/' denotes a cleavage site), and binds DNA as a monomer forming an asymmetric complex. In this complex a single catalytic center of BcnI contacts the scissile phosphodiester bond either on the 'C' (5′-CCCGG-3′) or the 'G' (5′-CCGGG-3′) DNA strand. Hence, to achieve a double strand break monomeric BcnI must perform a multi-step reaction: cut the first DNA strand, dissociate, re-bind the nicked recognition site in an opposite orientation, and then cleave the remaining DNA strand. Obligatory enzyme dissociation after the nicking step should result in accumulation of nicked products. Strikingly, only the final product with a double-strand break was observed in steady state DNA cleavage experiments (substrate excess conditions), indicating that BcnI cuts both DNA strands during a single association with the substrate DNA. On the other hand, single turnover (enzyme excess) reactions, initiated by addition of Mg^{2+} and a large excess of an inactive BcnI mutant to the preincubated wt enzyme and DNA, blocked cleavage of the second DNA strand. This suggested that after cleaving of the first DNA strand BcnI temporarily leaves the nicked recognition site, enabling binding of the inactive mutant. It was therefore hypothesized that re-orientation of BcnI should involve both sliding (1D diffusion along the DNA) and hopping (i.e. dissociation and re-binding to an adjacent site without excursions into bulk solution, as observed in (2,3)) (Figure 1). Typically, sliding, i.e. 1D diffu-

*To whom correspondence should be addressed. Tel: +370 5 2234365; Fax: +370 5 2234367; Email: siksnys@ibt.lt
Correspondence may also be addressed to Ralf Seidel. Tel: +49 341 97 32550; Email: ralf.seidel@physik.uni-leipzig.de
†These authors contributed equally to this work as first authors.

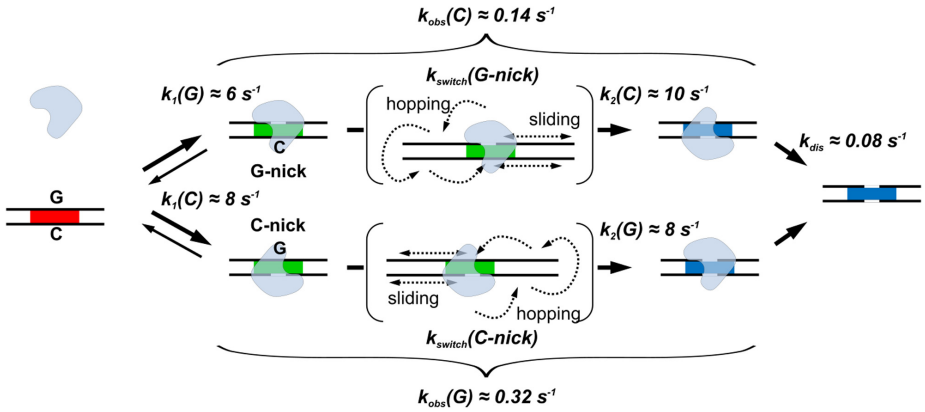

Figure 1. DNA cleavage by BcnI. The proposed DNA cleavage mechanism based on bulk kinetic studies of BcnI (7). It involves enzyme association (the lower limit for the bimolecular rate constant $3 \times 10^7\ M^{-1}\ s^{-1}$) at the asymmetric target site in either the 'G' orientation (the preferred binding mode, catalytic center close to the 'G' strand 5′-CCGGG-3′), or the 'C' orientation (catalytic center close to the 'C' strand 5′-CCCGG-3′), followed by rapid hydrolysis of the first DNA strand, slow cleavage of the second strand, and product release. The observed cleavage of the second strand [k_{obs}(C) and k_{obs}(G)] starts with a slow switch in the BcnI orientation [rate constants k_{switch}(G-nick) and k_{switch}(C-nick)], which presumably involves sliding and hopping of enzyme on the DNA, and a rapid hydrolysis reaction [k_2(C) and k_2(G)]. The major fraction of DNA (70–80%) is cleaved *via* the G-nick intermediate.

sion of the enzyme along the DNA driven by thermal forces, and hopping/jumping, i.e. dissociation of the enzyme from the DNA and re-binding at an adjacent/distant location, are considered as the major processes that help enzymes to locate their target sites among a large excess of non-specific DNA (4–6). BcnI, differently from other DNA enzymes, employs sliding and/or hopping as an integral part of the DNA cleavage reaction (7). Non-typical use of sliding has been reported before for the Type III REases, that employ ATP-triggered 1D diffusion in order to communicate between distant target sites on DNA (8,9). This, however, raises the question how these dynamic processes are integrated into an ATP-independent reaction pathway of BcnI.

Sliding and/or hopping of BcnI has been inferred from bulk kinetic measurements of DNA cleavage (7), but has not yet been directly observed. To monitor the dynamics of BcnI–DNA interactions, we employed different single molecule techniques. First, we monitored BcnI conformational changes in the absence and in the presence of DNA using confocal Förster resonance energy transfer (FRET) measurements. Next, we used a combination of total internal reflection fluorescence (TIRF) microscopy and magnetic tweezers to observe sliding and jumping of quantum dot-labeled enzyme on stretched nonspecific DNA. Finally, we characterized the dynamics and binding orientation of BcnI on cognate DNA using confocal and TIRF-based FRET measurements. Taken together, the single molecule data provide the first direct experimental support for the proposed BcnI sliding and jumping mechanism.

MATERIALS AND METHODS

DNA constructs

The 22.8 kb non-specific DNA constructs for BcnI sliding and jumping studies, the 7.4 kb DNA construct for cleavage measurements and the 135 and 535 bp DNA substrates with two BcnI sites for the bulk cleavage experiments were prepared as described in Supplementary Methods. Oligonucleotides used for PCR reactions are listed in Supplementary Table S1.

Mutagenesis and purification of BcnI proteins

Cysteine residues were introduced into selected positions by 'Quick Change' mutagenesis (10). Mutations were confirmed by sequencing the entire *bcnIR* gene. BcnI mutants were expressed and purified as described in (11). Proteins in the Storage Buffer (10 mM Tris–HCl pH 7.4 at 25°C, 0.2 M NaCl, 1 mM EDTA, 1 mM DTT, 50% glycerol) were stored at –20°C.

Production of fluorescently labeled BcnI proteins

Single-labeled BcnI. To remove glycerol and DTT, solution of the selected BcnI cysteine mutant in the Storage Buffer was diluted 2-fold with the labeling buffer (100 mM K-phosphate, 100 mM NaCl, 1 mM TCEP, pH 6.9 at 25°C), concentrated 10-fold using Amicon Ultra 10k centrifugal filters, and diluted 10-fold with the labeling buffer. This procedure was repeated five times. BcnI (20 μM) and the maleimide derivative of the fluorescent dye (10–20-fold molar excess) were incubated in the labeling buffer for 2 h at 25°C. The reaction was stopped by adding 40 μM 2-mercaptoethanol. The sample was loaded on a Heparin HP (GE Healthcare) column. Free dye was eluted with a 10 mM K-phosphate buffer (pH 7.0 at 25°C) containing 200 mM NaCl and 1 mM EDTA, and the protein–dye conjugate was eluted with a buffer containing 1 M NaCl. The labeled proteins were concentrated against the storage buffer and stored at –20°C. A similar procedure was performed to obtain biotinylated BcnI using BcnI(V105C+C202S) and maleimide–PEG_2–biotin (Thermo Fisher Scientific).

Double-labeled BcnI. To obtain double-labeled BcnI, the labeling was carried out in two steps. First, 100 μM BcnI(N18C+V105C+C202S) was mixed with 200 μM of Alexa488–C5–maleimide. Unlabeled protein, single-labeled

protein, and double-labeled protein were separately eluted from a Mono-S ion exchange chromatography column using a long (40 column volumes) 250–550 mM NaCl gradient. The single-labeled protein was used in the second labeling reaction with a 10-fold molar excess of Alexa546–C5–maleimide. The protein concentration and the labeling efficiency were measured by UV–vis absorption spectroscopy (Supplementary Methods). The fluorescence anisotropies (r) and the quantum yields (QY) of BcnI–dye conjugates were measured using fluorescence spectrometry. The Förster radii (R_0) for particular BcnI conjugates were calculated under various conditions (with and without Ca^{2+} and/or DNA) as described in Supplementary Methods. All determined labeling efficiencies and the values for r, QY and R_0 are listed in the Supplementary Table S2.

Confocal single-molecule FRET experiments

The studies of the binding orientation at the target site were performed using the single-labeled BcnI variants BcnI(N18C+C202S)–Alexa488, BcnI(V105C+C202S)–Alexa488 and BcnI(C202S–K209C)–Alexa488, as well as the single-labeled oligonucleotide duplexes Alexa546–C–DNA and Alexa546–G–DNA (Supplementary Table S1). 50 μl reactions contained 50 pM protein together with 50 pM oligoduplex in the Reaction Buffer (33 mM Tris–acetate, 66 mM K-acetate, pH 7.9 at 25°C) supplemented with 10 mM $Ca(OAc)_2$. The conformational states of BcnI were measured using 25–50 pM of double-labeled BcnI(N18C+V105C+C202S)–Alexa488–Alexa546 and 1–10 nM of specific (SP) and non-specific (NSP) DNA (Supplementary Table S1) in the reaction buffer with or without 10 mM $Ca(OAc)_2$. FRET measurements were performed using an inverted Zeiss LSM 780 confocal microscope equipped with a Confocor 3 unit allowing simultaneous dual-color fluorescence detection. Single BcnI–DNA complexes freely diffusing in solution were excited with a 488 nm laser (using the built in beam splitter MBS 488/561). The emission signal was simultaneously separated on a 'donor' and an 'acceptor' channel using a 565 nm dichroic mirror. The signals of the donor and the acceptor channels were additionally cleaned up using a 525 ± 30 nm band-pass filter and a 580 nm long-pass filter, respectively.

FRET data analysis

The FRET efficiency is defined as the rate of energy transfer from the donor to the acceptor divided by the rates of all processes that bring an excited donor back to the ground state. In confocal FRET measurements, the donor fluorophore is excited, and two fluorescence intensities are measured simultaneously: (i) the donor intensity I_{DD} (for donor excitation) and (ii) the acceptor intensity I_{DA} (for donor excitation). In order to obtain a real FRET efficiency (according to its definition) from the measured acceptor and donor intensities, one has to consider the non-specific fluorescent background (e.g. dark count rate, autofluorescence of sample cell, etc), the 'cross talk' between the donor and acceptor channels (correction factors α, β, see below), direct acceptor excitation (correction factor δ), and the different quantum yields of donor and acceptor fluorophores as well as different detection efficiencies (both combined in the correction factor γ) (12–14). Using background corrected intensities, the FRET efficiency was calculated according to:

$$E_{FRET} = \frac{(I_{DA} - \alpha * I_{DD}) - \gamma\delta\,(I_{DD} - \beta * I_{DA})}{(I_{DA} - \alpha * I_{DD}) + \gamma\,(I_{DD} - \beta * I_{DA})} \quad (1)$$

Obtained E_{FRET} values were plotted as histograms and multiple Gaussian distributions were fitted to the data. Fit results are summarized in Supplementary Table S4.

TIRF-based single-molecule FRET experiments

TIRF-based single-molecule FRET experiments were performed in the flow cells coated with biotinylated-polyethylene–glycol (15) with a combined magnetic tweezers–FRET instrument (16). Flow cell was incubated with 1 mg/ml streptavidin for 30 min, then washed with 1 ml of PBS buffer (2.7 mM KCl, 137 mM NaCl, 10 mM phosphate pH 7.4 at 25°C, Sigma) and with 200 μl of the measurement buffer (reaction buffer supplemented with 0.02 mg/ml glucose oxidase, 0.008 mg/ml catalase, 20 mM glucose, 0.1 mg/ml BSA, saturated TROLOX solution with 10 mM $Ca(OAc)_2$). 50 μl of 0.1 nM Cy5-labeled biotinylated DNA oligoduplexes (Supplementary Table S1) were incubated in the flow cell for 20 min to allow DNA attachment to the flow cell surface. Detached DNA was washed from the flow cell with 1 ml of PBS buffer and 200 μl of the Measurement Buffer. Positions of attached Cy5-labeled DNA molecules were determined by illuminating the flow cell with 43 mW 642 nm laser, the flow cell was illuminated with 50 mW 532 nm laser and 0.1–0.2 nM of BcnI (N18C+C202S)–Cy3–maleimide were injected. The emissions of the Cy3 and Cy5 fluorophores were spectrally separated using a 635 nm dichroic mirror and were projected on either half of the chip of an iXon 897-D EMCCD camera (Andor, Belfast, Ireland). The data collection was controlled using custom software written in LabView (National Instruments, Austin, United States). Single-molecule FRET traces were extracted from the fluorescence images with MATLAB (MathWorks, Natick, United States). 2D Gaussian distributions were fitted to Cy3 and Cy5 fluorescence signals that co-localize with the initially detected positions of DNA molecules and the obtained single-molecule FRET traces were corrected for the background and α, β, γ, δ correction factors.

Single-molecule observation of BcnI binding on stretched DNA

Single-molecule binding experiments on stretched DNA, including the flow cell preparation, the combined TIRF-magnetic tweezers setup and the data analysis have been previously described in detail (9). To enable prolonged observation of fluorescent enzyme molecules, experiments were performed using the BcnI(V105C+C202S)–maleimide–PEG2–biotin conjugate labeled with streptavidin-coated quantum dots (Qdot®625 streptavidin conjugate, diameter 15–20 nm, Molecular Probes, Life Technologies). Subsequent modification of BcnI(V105C+C202S) with PEG–biotin and quantum dots

reduced its activity in the steady-state DNA cleavage reactions ∼10-fold (Supplementary Table S3). This decrease in activity partially can be attributed to protein inactivation during the handling procedures, and adsorption of the quantum dot-labeled protein to surface of the vials in the activity measurement assays. The above problems should be less pronounced in the single-molecule experiments, where only the active BcnI molecules capable of DNA binding are observed; however, direct effect of the bulky quantum dot on the behavior and activity of BcnI cannot be fully excluded. The 22.8 kbp DNA construct devoid of BcnI sites (Supplementary Figure S1A) was preincubated with streptavidin-coated 1 μm magnetic beads (MyOne, ThermoFisher Scientific) and immobilized on the antidigoxigenin-covered bottom surface of the flow cell consisting of a capillary with a quadratic cross section (VitroCom). Subsequently, the DNA was stretched with a magnet in almost parallel orientation to the glass surface (Figure 3A). The small tilt angle arising from the attached magnetic bead was ∼5°, such that its influence on the measured enzyme displacement can be neglected. The sample was excited with a 488 nm laser in total internal reflection geometry at a power of 10 mW. After injection of 0.1–0.2 nM Qdot-labeled BcnI, the binding and diffusion events of single BcnI molecules on DNA were recorded. The measurements were carried out in the reaction buffer supplemented with 0.02 mg/ml glucose oxidase, 0.008 mg/ml catalase, 20 mM glucose, 0.1 mg/ml BSA and 14 mM 2-mercaptoethanol. The positions of individual BcnI molecules bound to DNA were obtained from raw image data using the FIESTA software (17). 1D diffusion coefficients were calculated from the mean square displacement of the enzyme position *vs* time plots (Figure 4A). Kymographs (Figure 3B) were generated using ImageJ (18).

Single molecule DNA hydrolysis assay

The single-molecule DNA nicking and cleavage assay was carried out using magnetic tweezers as previously described (8,19). Flow cells were incubated for 1 h with 50 μg/ml antidigoxigenin in PBS buffer (2.7 mM KCl, 137 mM NaCl, 10 mM phosphate pH 7.4 at 25°C, Sigma) followed by a 1 h incubation with 20 mg/ml BSA. After rinsing the flow cell with the PBS buffer, non-magnetic 3-μm polystyrene beads serving as a position reference (20) were applied to the flow cell and incubated for 30 min to allow their binding to the surface. Unbound reference beads were washed away using PBS. The 7.4 kb DNA construct (Supplementary Figure S1B) with biotinylated and digoxigenin-labeled termini was incubated with streptavidin-coated 1 μm magnetic beads (MyOne, ThermoFisher Scientific) and injected into the flow cell. Excess of unbound DNA molecules was washed out with PBS after 10 min, and DNA molecules were stretched using a pair of magnets mounted on a motorized stage above the flow cell (see (21) for details on the magnetic tweezers setup). The DNA length was inferred from the position of the magnetic bead above the flow cell surface. Bead positions were obtained using videomicroscopy (20,22). The force acting on the DNA molecule was obtained by power-spectral density analysis of the magnetic bead fluctuations perpendicular to the force (23). Individual DNA molecules held at a tension of 2 pN were positively supercoiled by applying 25 turns of the magnets. 0.2–1 nM BcnI(N18C+C202S) in the reaction buffer supplemented with 10 mM $Mg(OAc)_2$, 0.02 mg/ml glucose oxidase, 0.008 mg/ml catalase and 20 mM glucose in saturated TROLOX solution was injected into the flow cell and the DNA length was monitored. DNA nicking by BcnI resulted in an increase in DNA length due to its torsional relaxation. Upon cleavage of the second strand the bead was released (Figure 7A).

Bulk DNA cleavage experiments of a two-site DNA fragment

DNA cleavage experiments of the two-site DNA substrates (2 × CCSGG) were performed with 2 nM ^{33}P-labeled and 98 nM unlabeled di-hairpin 135 or 535 bp DNA substrates (Supplementary Figure S1C, Table S1). The DNA was mixed with 1 nM BcnI(wt) in the Reaction Buffer; the reactions were started by addition of 10 mM $Mg(OAc)_2$ and terminated at timed intervals by addition of the loading dye solution (75 mM EDTA, 0.01% bromphenol blue, 0.1% SDS, 50% (v/v) glycerol, pH 8.0). Reaction products were separated using polyacrylamide gel electrophoresis. The processivity of BcnI was estimated from the time course of the reaction products, i.e. uncut (SS), single cut (PS) and double-cut (PP) DNA forms (see Supplementary Methods).

RESULTS

Conformational states of BcnI

Several crystallographic structures are available for BcnI, including apo-BcnI (PDB ID: 2ODH) and BcnI in complex with cognate DNA (PDB IDs: 2ODI and 3IMB, with the BcnI active site close to the 'C' and the 'G' strands, respectively) (24). The structural data indicates that formation of the specific enzyme–DNA complex is accompanied by the transition of BcnI from the more open conformation to a more closed conformation. Upon formation of the closed structure, the DNA recognition and catalysis subdomains move closer to each other and lock DNA in the binding cleft (Figure 2A). To verify whether the conformations of BcnI in the crystals correlate with those in solution, and to assess how 'closed' the conformation of BcnI is when bound to non-specific DNA, we performed single molecule FRET experiments using BcnI variants carrying a pair of fluorescent labels (Alexa488 and Alexa546), one on each subdomain. Positions for both labels were selected such that the distance between the Cβ atoms of the corresponding residues (N18 and V105) is close to the theoretical R_0 value for the Alexa488–Alexa546 dye pair (6.4 nm), and the distance change upon the transition from the apo- ('open', PDB ID: 2ODH) to the DNA-bound ('closed', PDB ID: 2ODI, Figure 2A) form results in a significant change in FRET efficiency. To enable site-specific double labeling of BcnI, the sole native cysteine (C202) present in wt BcnI was replaced with a serine, and both N18 and V105 residues were replaced with cysteines. The resultant BcnI variant BcnI(N18+V105C+C202S) and its double-labeled derivative BcnI(N18+V105C+C202S)–Alexa488–Alexa546 (see Materials and Methods for details) were less active than

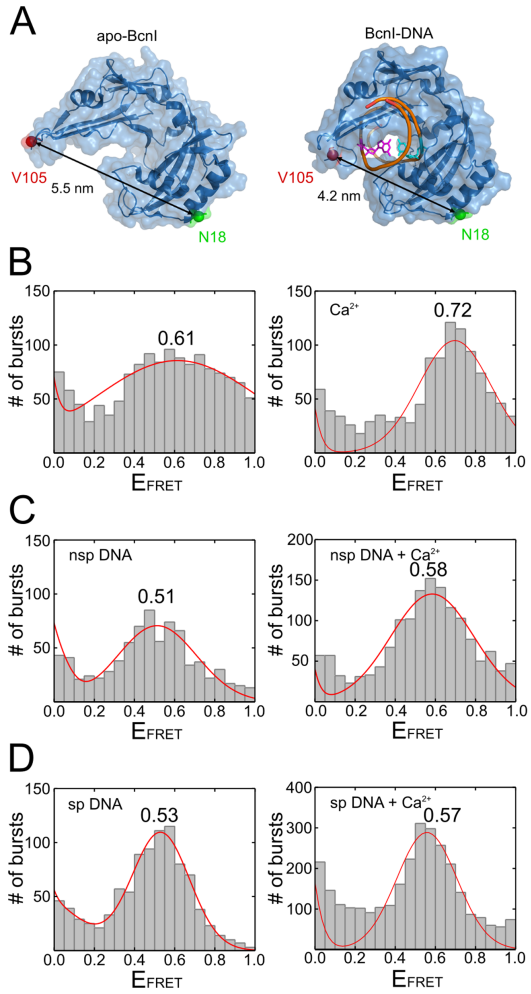

Figure 2. BcnI conformational dynamics in the absence and in the presence of DNA. (**A**) Structures of apo-BcnI (PDB ID 2ODH) (**A**) and the BcnI–DNA complex (PDB ID: 2ODI). The green and red spheres indicate the Cβ atoms of N18 and V105 residues used for fluorescent labeling. The transition of BcnI from the apo- ('open') to the DNA-bound ('closed') conformation reduces the distance between the Cβ atoms from 5.5 to 4.2 nm, causing an increase in FRET efficiency. The central G and C nucleotides of the BcnI target site are depicted in magenta and cyan, respectively. Single molecule FRET experiments were performed with double-labeled BcnI(N18C+V105C+C202S)–Alexa488–Alexa546 using a confocal microscope. FRET efficiency histograms obtained for double-labeled BcnI(N18C+V105C+C202S)–Alexa488–Alexa546 in the absence or presence of Ca^{2+} ions are shown for BcnI only (**B**), BcnI in the presence of non-specific DNA (**C**) and BcnI in the presence of specific DNA (**D**).

the wt protein as measured under steady-state conditions (Supplementary Methods, Supplementary Table S3), but they all retained the wt-like DNA cleavage pattern (direct conversion of supercoiled plasmid into the linearized form with no accumulation of nicked plasmid), and wt-like DNA binding ability (Supplementary Figures S2 and S3).

The single molecule FRET measurements on freely diffusing proteins were performed using an inverted confocal microscope using various assay conditions: without DNA, with non-specific (NSP) DNA, and with specific (SP) DNA, all in the absence and in the presence of Ca^{2+} ions (Figure 2B–D). In the absence of DNA and Ca^{2+} ions, the predominant fraction of BcnI is in a low FRET efficiency (E_{FRET}) state (0.61), and the E_{FRET} histogram is broad ($\sigma = 0.41$, Figure 2B and Supplementary Table S4), suggesting that under these conditions BcnI is flexible and exhibits no single defined conformational state. Alternatively, the flexible dye attachment could lead to such a broadening, which is however less likely due to narrower FRET distributions found at altered conditions (see below). Addition of NSP or SP DNA resulted in significantly narrower distributions for the E_{FRET} values ($\sigma = 0.2$), indicative of a more defined BcnI conformation, but the E_{FRET} values in both experiments remained close to 0.5 (0.51–0.53, Figure 2C and D). This is consistent with the lack of SP/NSP DNA discrimination by BcnI in the absence of divalent metal ions (Supplementary Figure S2). BcnI forms slightly more closed complexes with both DNAs in the presence of Ca^{2+} ($E_{FRET} = 0.57$, Figure 2C and D), albeit a narrower E_{FRET} distribution observed with SP DNA ($\sigma = 0.09$ for SP DNA versus 0.21 for NSP DNA) suggests that the conformation of BcnI with SP DNA is less flexible, i.e. better defined. Surprisingly, the highest E_{FRET} value of 0.72 was observed for apo-BcnI in the presence of Ca^{2+} (Figure 2B, Supplementary Table S4). Presumably, Ca^{2+} coordination by the negatively charged side chains in the DNA binding cleft brings the catalytic and recognition subdomains into close proximity. We note that the fluorescence anisotropies of single labeled BcnI (Supplementary Table S2) were not affected by the addition of Ca^{2+} suggesting that the conformational space of the dyes and the dye-protein interaction was not altered. However, based on distance error estimates using the so-called nanopositioning system (25) we cannot fully rule out that the change in the FRET efficiency is due to a change of the average relative dye orientation.

Dynamics of the non-cognate BcnI–DNA interactions

1D diffusion and jumping of single BcnI molecules on DNA. It was hypothesized that the flip of the BcnI orientation (Figure 1), which is required to complete the dsDNA cleavage reaction, involves sliding and/or hopping of the enzyme molecule on the nonspecific DNA surrounding the recognition site (7). To visualize the motion of individual BcnI molecules on stretched DNA molecules, and to determine the quantitative parameters for the dynamics of the BcnI-nonspecific DNA interactions, we employed a custom-built experimental setup, which combines total internal reflection fluorescence (TIRF) microscopy with magnetic tweezers (9). A 22.8 kbp DNA fragment devoid of BcnI recognition sequences was immobilized between the bottom surface of a flow cell and a magnetic bead. The magnetic tweezers were used to stretch the DNA construct laterally such that the DNA molecules were almost parallel to the glass surface. The binding and movement of individual quantum dot-labeled BcnI molecules was observed using the TIRF unit of the setup (see Materials and Methods for details) (Figure 3A). Enzyme binding resulted in the appearance of mobile diffraction limited fluorescence spots at random positions along the DNA. Two types of enzyme motion could be distinguished: continuous changes in protein position along the DNA axis, attributed to 1D diffusion of BcnI, and abrupt changes in enzyme position (≥100

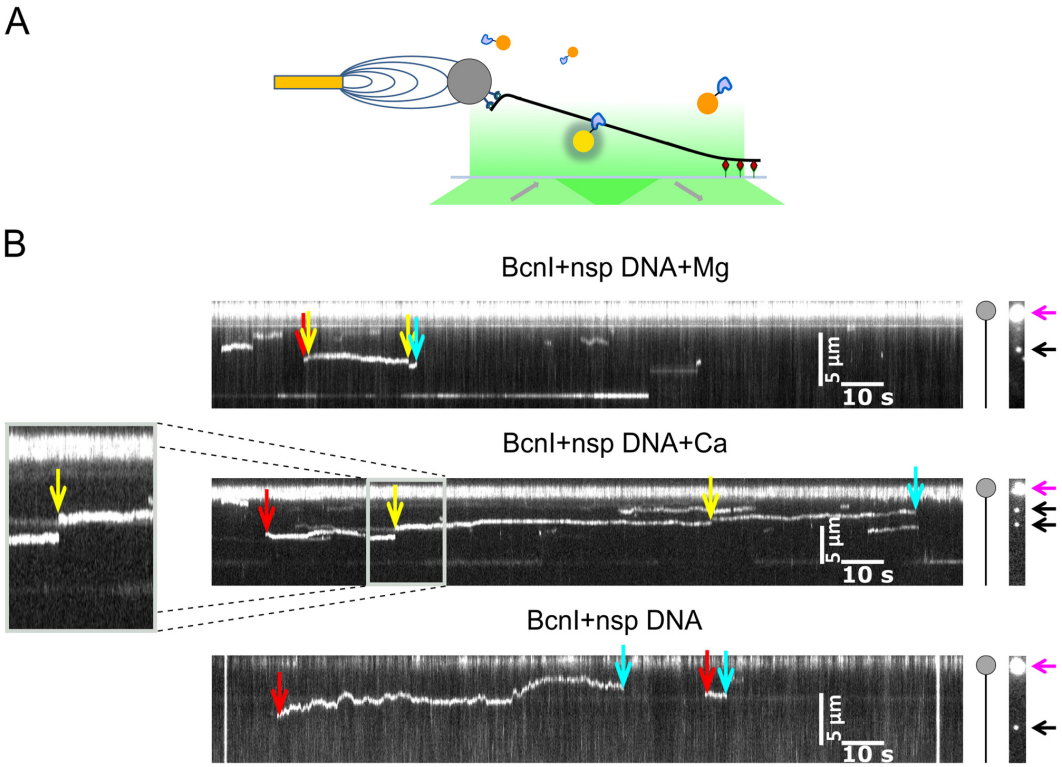

Figure 3. Observation of sliding and jumping of BcnI on DNA. (**A**) Experimental configuration. A 22.8 kb DNA molecule lacking BcnI recognition sites (black) was attached to a magnetic bead (grey sphere) and to the surface of a flow cell. The DNA was stretched sidewards using a magnet placed next to the flow cell. An evanescent field (green) of a TIRF-microscope was illuminating quantum-dot labeled enzymes bound to the DNA (yellow). Most of the freely diffusing enzymes in solution (orange) were outside of the evanescent field. (**B**) Representative kymographs of the movement of quantum-dot labeled BcnI on the DNA in the presence of Mg^{2+} ions (top) (straight horizontal line in the lower part of the kymograph depicts protein stuck on the surface of the flow cell), in the presence of Ca^{2+} ions (middle), and without divalent metal ions (bottom). Protein association, jumps, and protein dissociation are marked with red, green and blue arrows, respectively. Positions of the magnetic bead and fluorescent BcnI proteins are marked on the right-hand side with magenta and black arrows, respectively.

nm between two consecutive frames separated by 100 ms) that were interpreted as jumps (dissociation of BcnI and re-association with the DNA at a distant site). Taking into account the subnanomolar concentration of BcnI used in the experiments and the frequency of association of new BcnI molecules, arrival of a second BcnI molecule during a single time frame (100 ms) during the jump event is highly improbable. Such jumps were in detail investigated for the restriction enzyme EcoRV (26). They arise from the fact that an enzyme that dissociates from a DNA site has a high probability to rebind on the same DNA but on a distant site.

1D diffusion of BcnI on DNA was recorded in the absence of divalent metal ions, in the presence of Ca^{2+}, and in the presence of Mg^{2+} ions. In the absence of divalent cations diffusion events of BcnI appeared to be long-lived and without jumps. In contrast, in the presence of Mg^{2+} and Ca^{2+}, the diffusion events were shorter and frequently terminated by jumps or dissociation (Figure 3B).

From the time trajectories of enzyme position during diffusion on DNA, mean-square displacement (MSD) versus time plots were calculated and used to estimate the 1D diffusion coefficients (D_1) (Figure 4A). D_1 values for all conditions tested (Mg^{2+}, Ca^{2+}, no divalent cations) were in the order of 1×10^{-2} µm^2/s, with the highest value (1.7×10^{-2} µm^2/s) measured in the absence of divalent cations, and the lowest value (0.4×10^{-2} µm^2/s) measured in the presence of 10 mM Mg^{2+}. Due to the attached quantum dot that is quite large compared to the enzyme these obtained values represent lower bounds for the diffusion coefficient of the label-free enzyme. Assuming that the diffusion of BcnI is coupled to rotation along the helical pitch and a flexible attachment of the quantum dot, one can estimate the influence of the label (27). This provides 3.5-fold, 1.5-fold and 1.2-fold faster diffusion coefficients compared to the measured ones in absence of divalent ions and in presence of Ca^{2+} and Mg^{2+} respectively. We have also extracted the jump lengths (Figure 4B) and the 'sliding time', i.e. the time between two jumps or association/dissociation events. Without divalent metal ions BcnI diffuses on DNA on average 160 s; both Mg^{2+} and Ca^{2+} stimulate jumping and dissociation of BcnI to a similar extent, with jumps being observed approximately every 25 s (Mg^{2+}) and 20 s (Ca^{2+}). As predicted by theoretical work (28) and observed experimentally for the homodimeric REase EcoRV, short jumps occurred more frequently than long ones (26). On the other hand, relatively low activity of the quantum dot-labeled BcnI (Supplementary Table S3) indicates that some steps of BcnI reaction, including jumps, are likely to be influenced by the attached quantum dot. However, the fact that jumps do not occur in absence of divalent metal ions but do occur in presence of divalent

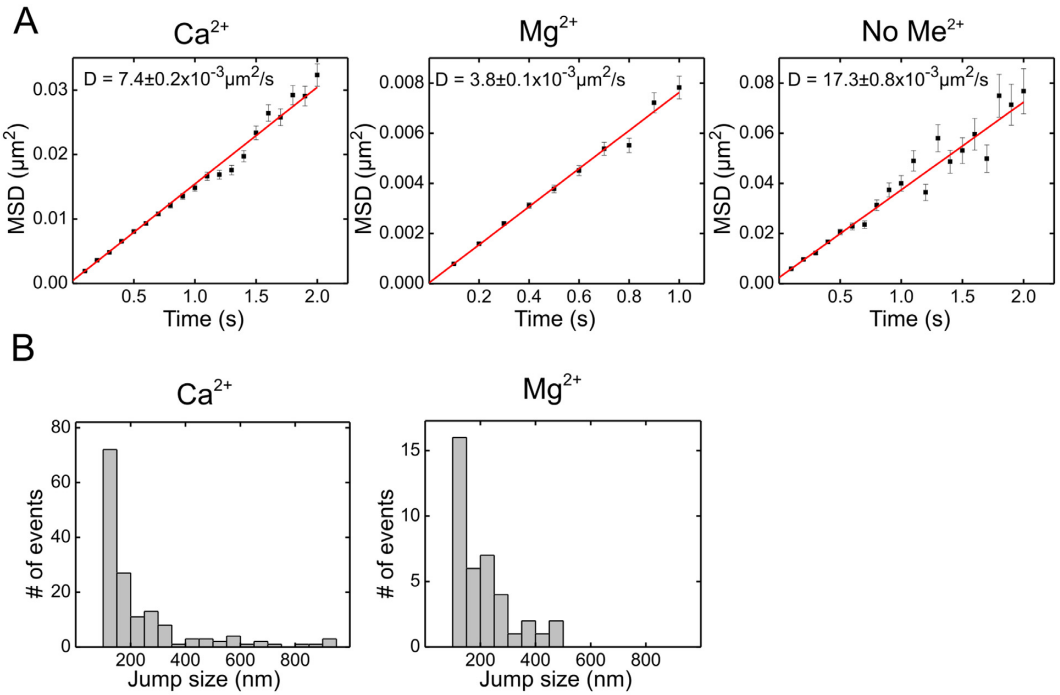

Figure 4. Sliding and jumping of BcnI on DNA. (**A**) Mean square displacements as a function of time for the motion of BcnI along DNA in the absence of divalent ions or in the presence of Ca^{2+} and Mg^{2+}. The diffusion constants D_1 were obtained from linear fits to the data at the shortest times (red lines). Number of analyzed traces was 102 for the experiment with Ca^{2+}, 44 for the experiment with Mg^{2+}, and 12 for the experiment with no divalent cations. (**B**) Jump size distribution of BcnI in the presence of Mg^{2+} and Ca^{2+}. Jumps in the absence of divalent ions were too rare to obtain statistically meaningful data.

metal ions provides a control that jumps are not induced by the label itself.

Processivity of BcnI. To obtain an independent estimate of the BcnI sliding length, we have also measured the processivity of BcnI, being defined as the ability of the enzyme to introduce two double-strand breaks on a two-site substrate during a single binding event (6). Previous bulk kinetic measurements performed on a two-site substrate with a short (10 bp) inter-site distance demonstrated that BcnI acts processively on closely located recognition sites (7). The extensive 1D diffusion of BcnI on dsDNA suggested that the processive action of BcnI could extend to longer inter-site distances. To further test the processivity of BcnI, we performed BcnI cleavage reactions on two-site DNA fragments with inter-site distances of either 100 or 500 bp (Supplementary Methods, Supplementary Figure S1C). Experiments were performed under steady-state reaction conditions with 100-fold substrate excess over the enzyme. Under these conditions any DNA product accumulating in the reaction mixture at the beginning of the reaction is in fact the final reaction product released by the enzyme (3). The maximal processivity of BcnI (equivalent to the fraction of DNA molecules cleaved at both sites during a single BcnI binding event) is expected to be 50%, since upon cleavage of the first recognition site there is only a 50% probability for BcnI to remain on the fragment with the second recognition site (the other 50% of BcnI will remain associated with the fragment devoid of the second recognition site, Supplementary Figure S3C). The processivity of BcnI was determined as $|v_{PP}/v_{SS}|$, i.e. the ratio of the initial rate for the formation of the double-cut product v_{PP} and of the total cleavage rate of the uncut substrate v_{SS} (see Supplementary information). It is thus the fraction of the double-cut products among all cleaved DNAs at early time points (3). The measured processivity approaches the theoretical maximum of 50%, when the diffusion of BcnI to the second recognition site and its subsequent cleavage is much faster than the dissociation from the fragment ($k_{cross} >> k_{diss}$). Considering the competition between these two processes, one can express the processivity as $50\% \times k_{cross}/(k_{cross} + k_{diss})$.

To gain insight into the processivity of BcnI, amounts of uncut, single cut (corresponding to the non-processive cleavage reaction) and double-cut (corresponding to the processive BcnI reaction) DNA forms (Supplementary Figure S3A) were quantified at different reaction time points and the processivity was determined from the ratio $|v_{PP}/v_{SS}|$ (Supplementary Figure S3B). We find that BcnI processively cuts ∼41–43% of both double-site fragments tested, indicating that k_{cross} is ∼4-fold higher than k_{diss}. Thus, BcnI is able to locate DNA sites 100 or 500 bp away from the search start position with high efficiency.

Site-specific BcnI–DNA interactions

BcnI orientation on DNA. BcnI recognizes the pseudopalindromic DNA recognition sequence 5′-CC(C/G)GG-3′. Being an asymmetric monomeric protein with a single catalytic site, BcnI can bind the recognition sequence in two orientations, i.e. by placing the catalytic center either in the vicinity of the 'C' (5′-CC<u>C</u>GG-3′)

strand (the 'C' binding orientation), or in the vicinity of the 'G' (5′-CCGGG-3′) strand (the 'G' binding orientation). Cleavage of double-stranded DNA by BcnI therefore must involve sequential binding of the enzyme in both orientations and cleavage of the corresponding DNA strands (Figure 1). Though the structures of both types of BcnI–DNA complexes were solved (PDB IDs: 2ODI and 3IMB) (Supplementary Figure S4), (24), bulk studies demonstrated that BcnI cleaves the majority of DNA *via* an intermediate with a nick in the 'G' strand, implying that the 'G' binding orientation is preferred by BcnI (7).

To test this prediction, we performed single molecule FRET measurements of freely diffusing protein–DNA complexes in a confocal detection scheme. The DNA was labeled with Alexa546 positioned 14 bp upstream of the recognition site on either the 'C' strand (oligoduplex Alexa546–C–DNA) or the 'G' strand (oligoduplex Alexa546–G–DNA, Supplementary Table S1), and BcnI was labeled with Alexa488. Dye positions on BcnI (N18, V105 and K209) were selected such that the flip in protein binding orientation from 'C' to 'G' would significantly change the distance between the C5 atom of the modified DNA pyrimidine base and the Cβ atom of the selected protein residue (the modelling was based on the BcnI–DNA structures 3IMB and 2ODI, Supplementary Figure S4). The corresponding BcnI mutants carrying a single cysteine residue at the desired position, and the theoretical E_{FRET} values calculated for both protein orientations are listed in Figure 5 and Supplementary Figure S5.

Measurements with BcnI(N18C+C202S)–Alexa488 and Alexa546–C–DNA revealed two E_{FRET} populations: a less abundant with a low FRET efficiency ($E_{FRET} = 0.35$) and a more abundant with a high FRET efficiency ($E_{FRET} = 0.69$, Figure 5A). Both values were in agreement with the theoretically expected FRET efficiencies for protein binding to the Alexa546–C–DNA in the 'C' and 'G' orientations of 0.27 and 0.61, respectively (Figure 5A) when assuming a dipole orientation factor of 2/3 (see Supplementary methods for limitations of this assumption). The opposite distribution was observed for the Alexa546–G–DNA, where the low E_{FRET} state (0.26) was more populated, and the high E_{FRET} state (0.62) was less populated, both values in good agreement with the expected values of 0.23 and 0.61 (Figure 5B). Thus, the single molecule FRET data obtained with both DNAs is consistent with a preferential binding of BcnI to DNA in the 'G' orientation. This conclusion is also supported by data obtained with other fluorescently labeled BcnI mutants (Supplementary Figure S5, Table S4).

Dynamics of site-specific BcnI–DNA interactions. According to bulk kinetic measurements, BcnI rapidly localizes its specific recognition site (the lower limit for the bimolecular rate constant is 3×10^8 M^{-1} s^{-1}), followed by rapid cleavage of the first strand (first-order rate constant ~7 s^{-1}), and a subsequent slow cut of the second DNA strand (observed rate constant ~0.15–0.3 s^{-1} (7)). The latter reaction stage must involve enzyme dissociation from the nicked intermediate, a switch in enzyme orientation, and DNA hydrolysis itself (Figure 1). Rapid cleavage of the pre-nicked DNA by BcnI (first-order rate constant approximately equal to 10 s^{-1}) suggested that the rate-limiting step of the second DNA strand cleavage is enzyme dissociation from the nicked DNA. To probe the residence time of BcnI for specific DNA interactions at the single molecule level, we employed a custom-built setup, which supports objective-type TIRF microscopy with simultaneous dual-color FRET detection (16). Cy5-labeled 36 bp DNA oligoduplexes (Supplementary Table S1) were attached to the bottom surface of a flow cell and positions of the attached fluorescent oligoduplexes were determined by short illumination (2 s) with a 642 nm laser. Upon injection of Cy3-labeled BcnI (final concentration 0.2 nM) into the flow cell, the BcnI–Cy3 conjugates were excited with a 532 nm laser (see Materials and Methods for details). Association of the Cy3-labeled BcnI with Cy5-labeled DNA correlated with a significant increase of fluorescence intensity in both the donor and the acceptor channels, where the signal in the acceptor channel is due to FRET between BcnI and DNA (Figure 6A). The FRET signal was used to discriminate protein binding to the DNA from non-specific protein-surface interactions. The durations of the events with significant FRET (apparent $E_{FRET} > 0.1$) in the presence of Ca^{2+} (Ca^{2+} supports specific DNA binding but not cleavage by BcnI) were best described by a double exponential distribution indicative of two types of BcnI–DNA complexes (see cumulative duration distributions in Figure 6B). The binding events with short residence times (mean duration: 0.35 s) were more frequent (70% of all events) than events with the long res-

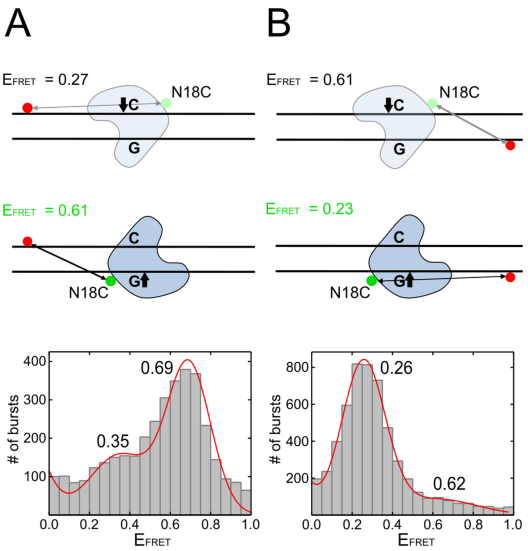

Figure 5. Preferred binding orientation of BcnI. Single molecule FRET experiments were performed with Alexa488-labeled BcnI(N18C+C202S) and Alexa546-labeled DNA. (**A**) FRET efficiency histogram obtained for 'C' strand-labeled DNA. Based on the available structures of BcnI–DNA complexes (PDB IDs: 2ODI and 3IMB), the expected distance between the Alexa488 (green sphere) and Alexa546 (red sphere) dyes is 71.3 and 56.2 Å for the different orientations of the protein–DNA complexes. This is equivalent to FRET efficiencies of 0.27 and 0.61 for protein bound in the 'C' and 'G' orientations, respectively (see sketches at the top). A double-Gaussian fit to the FRET efficiency data (red line) is consistent with preferred binding of BcnI in the 'G' orientation. (**B**) FRET efficiency histogram obtained for 'G' strand-labeled DNA. The expected FRET efficiencies are 0.61 and 0.23 for protein bound in the 'C' and 'G' orientations, respectively (see sketches at the top). As with the 'C' strand-labeled DNA, the experimental data is consistent with the preferential binding in the 'G' orientation.

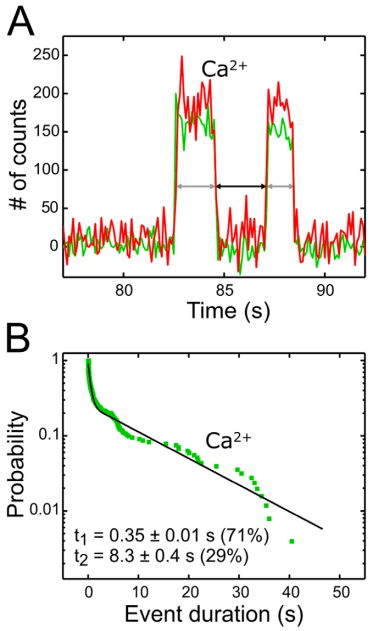

Figure 6. Dynamics of BcnI binding to its target site. Single molecule TRIF-based FRET experiments using surface-tethered 36 bp long Cy5-labeled DNA and Cy3-labeled BcnI(N18C+C202S). (**A**) Time trajectory of donor and acceptor fluorescence measured on a single DNA in the presence of Ca^{2+}. Arrows indicate the event duration times. (**B**) Cumulative distribution of the measured event durations. Double exponential fit to the data is shown as a solid line. Fit parameters are given next to the plot.

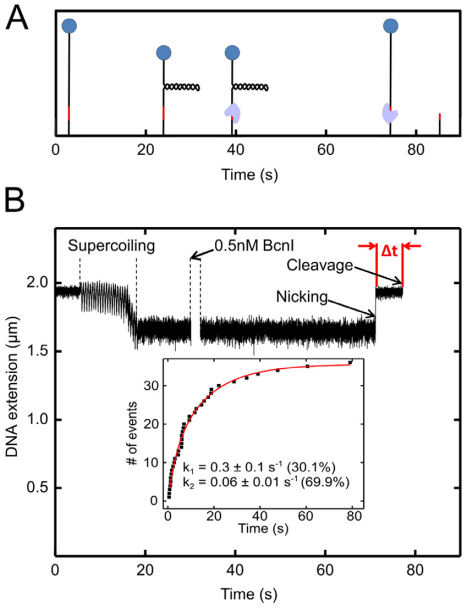

Figure 7. DNA cleavage by BcnI. (**A**) Scheme of the experiment. A 7.4 kb DNA fragment with a single BcnI recognition site was attached to the flow cell surface and a magnetic bead. The DNA was held stretched at 2 pN force and supercoiled with +25 turns. Subsequently, 0.2–1 nM BcnI was added. DNA nicking recovered the initial DNA length and cleavage of the second DNA strand released the bead. The time interval Δt between these two events is the lifetime of the nicked intermediate, or the inverse of the second DNA strand cleavage rate. (**B**) Experimental results. The cumulative distribution of the measured Δt values is shown in the inset. A double-exponential fit yielded $k_{obs}(1) = 0.3 \pm 0.1\ s^{-1}$ (30% events) and $k_{obs}(2) = 0.06 \pm 0.01\ s^{-1}$ (70% events).

idence times (mean duration: 8.3 s). Presumably, the short residence time of BcnI on the DNA corresponds to non-specific enzyme–DNA complexes (target search intermediates), while longer residence times correspond to specific enzyme–DNA interactions.

Kinetics of the DNA second strand cleavage. To directly assess the time required for a BcnI molecule to change its orientation on the recognition site after nicking of the first target strand, we employed magnetic tweezers to measure DNA cleavage (19,29). Different termini of the 7.4 kb DNA construct with a single BcnI recognition site were attached to the bottom surface of a flow cell and a magnetic bead. Using a pair of magnets placed above the flow cell the DNA was held stretched at a tension of 2 pN, while being positively supercoiled. Introduction of 25 positive turns reduced the length of the DNA construct due to formation of a plectonemic superhelix (Figure 7A). Two events were observed upon addition of BcnI: first, the full DNA length was recovered due to nicking of the first strand, followed by the disappearance of the bead due to cleavage of the second DNA strand (Figure 7B). The cumulative distribution of time intervals between the first and the second strand nicking was fitted with a double-exponential function, yielding rate constants for the second strand cleavage $k_{obs}(1) = 0.3 \pm 0.1\ s^{-1}$ (30% of cleavage events) and $k_{obs}(2) = 0.06 \pm 0.01\ s^{-1}$ (70% of cleavage events) (Figure 7B inset).

DISCUSSION

Kinetic studies in bulk solution suggested that the BcnI reaction mechanism consists of target site localisation, cleavage of the first strand, a switch in enzyme orientation *via* sliding and hopping, and cleavage of the second DNA strand (Figure 1). However, some stages of this mechanism, e.g. the interaction dynamics of BcnI with cognate and non-cognate DNA remained uncharacterized, while others, e.g. the sliding and hopping of the enzyme on the DNA, remained hypothetic. In the present study, we have attempted to characterize different BcnI reaction steps employing different single-molecule techniques.

Conformational states of BcnI

In the available apo-structure BcnI adapts the 'open' conformation, with the DNA binding and catalytic subdomains located relatively far apart, while in the DNA-bound structures the enzyme is present in the 'closed' form, with the two subdomains encircling the DNA (24) (Figure 2A). To check if these conformations also persist in solution, we have engineered double-labeled BcnI variants carrying Alexa488 and Alexa546 dyes on different subdomains. By measuring the FRET efficiencies at the single molecule level, we were able to discriminate BcnI molecules with different inter-subdomain distances (Figure 2B–D). In the presence of cognate DNA, most BcnI molecules adopt a higher-E_{FRET} state that is consistent with the 'closed' enzyme conforma-

tion (recognition/catalysis subdomains are in close proximity, Figure 2D). This finding is in good agreement with the available DNA-bound structures. Interestingly, a similar distribution was also observed for non-specific DNA (Figure 2C), suggesting that during target search (sliding), BcnI encircles the DNA in a similar way as in the specific complex. A broader distribution of the higher-E_{FRET} peak in this case suggests that the non-specific complex is more flexible than the specific complex. In contrast, in the absence of DNA and divalent metal ions, we observed a broad distribution of FRET efficiencies, indicative of a highly flexible protein lacking a defined conformation (Figure 2B). While the lower-E_{FRET} part of the distribution should be attributed to the 'open' BcnI conformation observed in the apo-structure, the higher-E_{FRET} part suggests that a comparable fraction of BcnI molecules adopt a more closed conformation, reminiscent of the DNA-bound structure. Addition of divalent metal ions to the BcnI–DNA complexes resulted in narrow higher-E_{FRET} distributions, indicative of tighter BcnI–DNA complexes. Unexpectedly, upon addition of Ca^{2+} to apo–BcnI, a large fraction of the enzyme also adopted the 'closed' conformation (Figure 2B). We presume that such compaction of enzyme structure could be induced by neutralization of the negative charges present on the DNA-binding surface of BcnI, in particular in the catalytic center. Though 'closed' apo–BcnI state might be incompatible with DNA binding, it must be in rapid equilibrium with more 'open' (lower E_{FRET}) BcnI states capable of DNA binding.

1D diffusion of BcnI along DNA

Using a combination of magnetic tweezers and TIRF microscopy, we were able to follow 1D diffusion (sliding) and 3D diffusion (jumping) of individual Qdot-labeled BcnI molecules on non-cognate DNA. We found that the diffusion coefficient D_1 for 1D sliding of BcnI on the DNA is 1.7×10^{-2} $\mu m^2/s$ in the absence of divalent metal ions, 0.8×10^{-2} $\mu m^2/s$ in the presence of 10 mM Ca^{2+}, and 0.4×10^{-2} $\mu m^2/s$ in the presence of 10 mM Mg^{2+} (Figure 4A). 1D diffusion constants in the order of 1×10^{-2} $\mu m^2/s$ were also reported for other DNA-interacting enzymes (26,27,30–38). D_1 is at least 1000-fold lower than the calculated 3D diffusion coefficient D_3 of the Qdot-labeled BcnI (30 $\mu m^2/s$) (6,39). This drastic reduction, also observed for other DNA-acting enzymes (26), can be attributed to the friction of the DNA–protein interactions during the sliding process (40) as well as in part to the hydrodynamics of the quantum-dot conjugated enzyme during its helical path around the DNA helix (41,42). Slower diffusion in the presence of divalent metal ions correlates with the more closed BcnI conformation observed in the presence of Ca^{2+} and DNA (Figure 2B and D). Tighter contacts between enzyme and non-cognate DNA may be required for probing the DNA sequence and recognition of the cognate site.

3D jumps of BcnI

Current theoretical and experimental studies indicate that target site localization by site-specific proteins involves both 1D sliding along the DNA, which allows probing of all DNA sites in the scanned region, and 3D hops/jumps, which relocate the protein to a nearby or a distant DNA site. An interplay of 1D and 3D diffusion may significantly accelerate target site location in comparison to a simple 3D search (6).

Along with protein sliding, our single molecule diffusion experiments revealed sudden translocations of BcnI on the DNA with a length of 100–1000 nm between two consecutive time frames (100 ms) (Figures 3B and 4B). Such protein movements would require a diffusion coefficient of 0.1–10 $\mu m^2/s$, which is significantly higher than the 1D diffusion coefficient D_1 discussed above (26). We therefore attribute these BcnI movements to 3D jumps on the DNA. Intriguingly, we find that the jump frequency is significantly lower in the absence of divalent metal ions (on average, one $\geq$100 nm translocation every 160 s) than in the presence of Ca^{2+} and Mg^{2+} (one translocation every 20–25 s, Figure 3B), indicating that metal ions facilitate enzyme dissociation from the DNA. As with EcoRV (26,43), the jump frequency decreased with the jump length (Figure 4B). Due to the spatial resolution of our experimental setup, jumps shorter than 100 nm could not be detected, but their frequency could be estimated using a theoretical model developed by Kolesov *et al.*, stating that each jump is on average accompanied by approximately five hops (i.e. jumps shorter than 50 nm, a single DNA persistence length) (28). This gives us the upper estimate for the average BcnI sliding duration, 30 (150/5) s in the absence of divalent metal ions, and 4 (20/5) s in the presence of Ca^{2+}/Mg^{2+}. Given the experimentally determined 1D diffusion coefficients, the average BcnI sliding length [$l_{sl} = (2D_1 \cdot t)^{0.5}$] in the absence of divalent metal ions is approximately equal to 1000 nm or 3500 bp, and up to 200 nm or 700 bp in the presence of Mg^{2+} or Ca^{2+}. Note that the sliding length could be up to 2-fold longer for a quantum dot free BcnI, given the smaller hydrodynamic radius of the unlabeled protein (27). Moreover, attachment of the large label significantly decreased the catalytic activity of BcnI (Supplementary Table S3), and therefore could also affect the jumping behavior of the enzyme. However, experiments in the absence of divalent metal ions (prolonged sliding events with almost no jumps, Figure 3B) argue against any artefactual jumps caused by the quantum dot. Moreover, the sliding distance of BcnI estimated here is consistent with the high processivity of BcnI on DNA substrates with inter-site distances as large as 500 bp (Supplementary Figure S2).

According to Halford and Marko (6), acceleration of the target site localization rate (k_a) beyond the diffusion-limited value ($D_3 \cdot a$) is expressed by Eq. (2):

$$\frac{k_a}{D_3 a} = \left(\frac{a}{l_{sl}} + \frac{D_3}{D_1} a L l_{sl} c \right)^{-1} \quad (2)$$

Assuming $a = 1.7$ nm (length of the 5 bp BcnI recognition site), $L = 1000$ nm (length of a 3000 bp DNA fragment), $c = 1 \times 10^{-10}$ nm^{-3} (0.1 nM target site concentration expressed as the number of molecules per cubic nanometer), and using the sliding length (l_{sl}) and diffusion coefficients (D_1, D_3) estimated in the present study, a significant acceleration in the presence of divalent metal ions of 3- to 8-fold

is obtained. Intriguingly, divalent metal ions seem to play a dual role in the nonspecific BcnI–DNA interactions: they decrease the 1D diffusion coefficient D_1 (presumably due to tighter protein–DNA interactions in the presence of divalent ions), and simultaneously increase the protein dissociation rate (or jumping frequency). Currently, we have no structural or mechanistic model accounting for this result.

Dynamics of BcnI–DNA interactions with cognate substrates

To directly measure the residence time of BcnI on specific DNA we have employed a custom-built single-molecule setup, which allowed us to detect individual association events between Cy3-labeled BcnI and Cy5-labeled 36 bp DNA (Figure 6A). Experiments in the presence of Ca^{2+} revealed two populations of events: 70% were short-lived (mean duration 0.35 s), and 30% long-lived (mean duration 8 s). We attribute two types of binding events to non-specific (short residence time) and specific (long residence time) BcnI–DNA complexes. The lifetime of the non-specific BcnI–DNA complexes observed in this experiment (0.35 s) is much shorter than the average BcnI sliding duration measured in the TIRF-magnetic tweezers setup (see above). Most likely, a shorter residence time of BcnI on non-specific DNA is due to the short length (36 bp) of DNA substrates, which enables the enzyme to slide off the DNA.

Second DNA strand cleavage by BcnI

The most intriguing BcnI reaction step is cleavage of the second DNA strand (Figure 1). It must involve enzyme dissociation from the nicked intermediate, rebinding in the opposite orientation, and cleavage of the second strand (7). Here, we have measured the second DNA strand cleavage rate employing magnetic tweezers (Figure 7). In this setup, DNA nicking results in relaxation of the plectonemic supercoil, and cleavage of the second DNA strand releases the magnetic bead. The time between these two events Δt includes several reaction steps: enzyme dissociation from the nicked intermediate, the orientation flip and cleavage of the second strand. The cumulative plot of Δt values followed a double-exponential function, an indication of two populations of DNA cleavage events with $k_{obs}(1) = 0.3 \pm 0.1\ s^{-1}$ (30% events), and $k_{obs}(2) = 0.06 \pm 0.01\ s^{-1}$ (70% events, Figure 7, inset). These values are in good agreement with the second DNA strand cleavage rates determined from bulk kinetics, the rate constant k_{obs}(G) for cleavage of the 'G' strand in the 'C-nick' intermediate (0.32 s^{-1}, 30% of all DNA), and the rate constant k_{obs}(C) for cleavage of the 'C' strand in the 'G-nick' intermediate (0.14 s^{-1}, 70% of all DNA) (7). Thus, the slower cleavage events [$k_{obs}(2)$] observed in the single molecule setup may correspond to the predominant (70%) DNA cleavage pathway, where 'C' strand is cleaved after the 'G' strand, and the more rapid cleavage events [$k_{obs}(1)$] may correspond to the alternative (30%) pathway, where the cleavage order is reversed. The dominance of the 'G-nick' pathway in bulk kinetics (7) was attributed to preferential binding of BcnI to DNA in an orientation that places the catalytic center close to the 'G' strand. We now confirm this BcnI binding preference using single molecule FRET measurements with labeled BcnI and DNA (Figure 5 and Supplementary Figure S5).

The second strand cleavage rate k_{obs} can be expressed by equation (3).

$$\frac{1}{k_{obs}} = \frac{1}{k_{dissoc}} + \frac{1}{k_{flip}} + \frac{1}{k_{chem}} \quad (3)$$

where k_{dissoc}, k_{flip} and k_{chem} are the rate constants for enzyme dissociation from nicked DNA, re-binding and DNA hydrolysis, respectively. Since the hydrolysis step k_{chem} is rapid, 8–10 s^{-1} (7), and we show here that BcnI jumps on the DNA take <0.1 s (Figure 3B), the rate limiting step for k_{obs}, must be k_{dissoc}, i.e. slow dissociation of BcnI from the nicked intermediate. Different k_{obs} values observed for the 'G-nick' and 'C-nick' reaction pathways must therefore reflect different enzyme dissociation rates from the 'G-nick' and the 'C-nick' intermediates. Here, slower dissociation from the 'G-nick' intermediate prior to 'C' strand cleavage correlates with tighter enzyme binding in the 'G' orientation.

Taken together, we have performed a thorough study of the monomeric restriction enzyme BcnI–DNA interactions, employing a diverse set of single molecule techniques. This allowed us to characterize reaction steps that are difficult or impossible to access using conventional techniques, for example, direct observation of 1D diffusion and jumping of the protein on the DNA, protein binding orientation and conformational dynamics, and dynamics of specific and non-specific protein–DNA interactions. Our results are consistent with the BcnI reaction mechanism proposed from bulk solution studies, and provide additional mechanistic details, such as enzyme–DNA dissociation times, sliding length and jumping frequency of the protein. The set of single-molecule techniques described here could be successfully applied to other DNA-interacting proteins.

SUPPLEMENTARY DATA

Supplementary Data are available at NAR Online.

ACKNOWLEDGEMENTS

Authors acknowledge Wolfgang Staroske for support with the confocal FRET measurements and Sihwa Joo for the initial TIRF-based measurements.

FUNDING

European Research Council [GA 261224 to R.S.]; Research Council of Lithuania [KEL-11460 and DOC-13060 to G.K.]; European Union Research Potential Call FP7-REGPOT-2009-1 [245721 'MoBiLi' project]. Funding for open access charge: Research Council of Lithuania.
Conflict of interest statement. None declared.

REFERENCES

1. Roberts,R.J., Vincze,T., Posfai,J. and Macelis,D. (2015) REBASE–a database for DNA restriction and modification: enzymes, genes and genomes. *Nucleic Acids Res.*, **43**, D298–D299.
2. Halford,S.E. (2009) An end to 40 years of mistakes in DNA-protein association kinetics? *Biochem. Soc. Trans.*, **37**, 343–348.
3. Gowers,D.M., Wilson,G.G. and Halford,S.E. (2005) Measurement of the contributions of 1D and 3D pathways to the translocation of a protein along DNA. *Proc. Natl. Acad. Sci. U.S.A.*, **102**, 15883–15888.

4. Berg,O.G., Winter,R.B. and von Hippel,P.H. (1981) Diffusion-driven mechanisms of protein translocation on nucleic acids. 1. Models and theory. *Biochemistry*, **20**, 6929–6948.
5. Shimamoto,N. (1999) One-dimensional diffusion of proteins along DNA. Its biological and chemical significance revealed by single-molecule measurements. *J. Biol. Chem.*, **274**, 15293–15296.
6. Halford,S.E. and Marko,J.F. (2004) How do site-specific DNA-binding proteins find their targets? *Nucleic Acids Res.*, **32**, 3040–3052.
7. Sasnauskas,G., Kostiuk,G., Tamulaitis,G. and Siksnys,V. (2011) Target site cleavage by the monomeric restriction enzyme BcnI requires translocation to a random DNA sequence and a switch in enzyme orientation. *Nucleic Acids Res.*, **39**, 8844–8856.
8. Ramanathan,S.P., van Aelst,K., Sears,A., Peakman,L.J., Diffin,F.M., Szczelkun,M.D. and Seidel,R. (2009) Type III restriction enzymes communicate in 1D without looping between their target sites. *Proc. Natl Acad. Sci. U.S.A.*, **106**, 1748–1753.
9. Schwarz,F.W., Toth,J., van Aelst,K., Cui,G., Clausing,S., Szczelkun,M.D. and Seidel,R. (2013) The helicase-like domains of type III restriction enzymes trigger long-range diffusion along DNA. *Science*, **340**, 353–356.
10. Zheng,L., Baumann,U. and Reymond,J.-L. (2004) An efficient one-step site-directed and site-saturation mutagenesis protocol. *Nucleic Acids Res.*, **32**, e115.
11. Kostiuk,G., Sasnauskas,G., Tamulaitiene,G. and Siksnys,V. (2011) Degenerate sequence recognition by the monomeric restriction enzyme: single mutation converts BcnI into a strand-specific nicking endonuclease. *Nucleic Acids Res.*, **39**, 3744–3753.
12. Hohlbein,J., Craggs,T.D. and Cordes,T. (2014) Alternating-laser excitation: single-molecule FRET and beyond. *Chem. Soc. Rev.*, **43**, 1156–1171.
13. Gust,A., Zander,A., Gietl,A., Holzmeister,P., Schulz,S., Lalkens,B., Tinnefeld,P. and Grohmann,D. (2014) A starting point for fluorescence-based single-molecule measurements in biomolecular research. *Molecules*, **19**, 15824–15865.
14. Theissen,B., Karow,A.R., Köhler,J., Gubaev,A. and Klostermeier,D. (2008) Cooperative binding of ATP and RNA induces a closed conformation in a DEAD box RNA helicase. *Proc. Natl. Acad. Sci. U.S.A.*, **105**, 548–553.
15. Roy,R., Hohng,S. and Ha,T. (2008) A practical guide to single-molecule FRET. *Nat. Methods*, **5**, 507–516.
16. Kemmerich,F.E., Swoboda,M., Kauert,D.J., Grieb,M.S., Hahn,S., Schwarz,F.W., Seidel,R. and Schlierf,M. (2015) Simultaneous single-molecule force and fluorescence sampling of DNA nanostructure conformations using magnetic tweezers. *Nano Lett.*, doi:10.1021/acs.nanolett.5b03956.
17. Ruhnow,F., Zwicker,D. and Diez,S. (2011) Tracking single particles and elongated filaments with nanometer precision. *Biophys. J.*, **100**, 2820–2828.
18. Schneider,C.A., Rasband,W.S. and Eliceiri,K.W. (2012) NIH Image to ImageJ: 25 years of image analysis. *Nat. Methods*, **9**, 671–675.
19. van Aelst,K., Tóth,J., Ramanathan,S.P., Schwarz,F.W., Seidel,R. and Szczelkun,M.D. (2010) Type III restriction enzymes cleave DNA by long-range interaction between sites in both head-to-head and tail-to-tail inverted repeat. *Proc. Natl. Acad. Sci. U.S.A.*, **107**, 9123–9128.
20. Huhle,A., Klaue,D., Brutzer,H., Daldrop,P., Joo,S., Otto,O., Keyser,U.F. and Seidel,R. (2015) Camera-based three-dimensional real-time particle tracking at kHz rates and Ångström accuracy. *Nat. Commun.*, **6**, 5885.
21. Kemmerich,F.E., Kasaciunaite,K. and Seidel,R. (2016) Modular magnetic tweezers for single-molecule characterizations of helicases. *Methods*, doi:10.1016/j.ymeth.2016.07.004.
22. Otto,O., Czerwinski,F., Gornall,J.L., Stober,G., Oddershede,L.B., Seidel,R. and Keyser,U.F. (2010) Real-time particle tracking at 10,000 fps using optical fiber illumination. *Opt. Express*, **18**, 22722.
23. Daldrop,P., Brutzer,H., Huhle,A., Kauert,D.J. and Seidel,R. (2015) Extending the range for force calibration in magnetic tweezers. *Biophys. J.*, **108**, 2550–2561.
24. Sokolowska,M., Kaus-Drobek,M., Czapinska,H., Tamulaitis,G., Szczepanowski,R.H., Urbanke,C., Siksnys,V. and Bochtler,M. (2007) Monomeric restriction endonuclease BcnI in the apo form and in an asymmetric complex with target DNA. *J. Mol. Biol.*, **369**, 722–734.
25. Muschielok,A., Andrecka,J., Jawhari,A., Brückner,F., Cramer,P. and Michaelis,J. (2008) A nano-positioning system for macromolecular structural analysis. *Nat. Methods*, **5**, 965–971.
26. Bonnet,I., Biebricher,A., Porté,P.-L., Loverdo,C., Bénichou,O., Voituriez,R., Escudé,C., Wende,W., Pingoud,A. and Desbiolles,P. (2008) Sliding and jumping of single EcoRV restriction enzymes on non-cognate DNA. *Nucleic Acids Res.*, **36**, 4118–4127.
27. Dikic,J., Menges,C., Clarke,S., Kokkinidis,M., Pingoud,A., Wende,W. and Desbiolles,P. (2012) The rotation-coupled sliding of EcoRV. *Nucleic Acids Res.*, **40**, 4064–4070.
28. Kolesov,G., Wunderlich,Z., Laikova,O.N., Gelfand,M.S. and Mirny,L.A. (2007) How gene order is influenced by the biophysics of transcription regulation. *Proc. Natl. Acad. Sci. U.S.A.*, **104**, 13948–13953.
29. Rutkauskas,M., Sinkunas,T., Songailiene,I., Tikhomirova,M., Siksnys,V. and Seidel,R. (2015) Directional R-loop formation by the CRISPR-cas surveillance complex cascade provides efficient off-target site rejection. *Cell Rep.*, **10**, 1534–1543.
30. Harada,Y., Funatsu,T., Murakami,K., Nonoyama,Y., Ishihama,A. and Yanagida,T. (1999) Single-molecule imaging of RNA polymerase-DNA interactions in real time. *Biophys. J.*, **76**, 709–715.
31. Wang,Y.M., Austin,R.H. and Cox,E.C. (2006) Single molecule measurements of repressor protein 1D diffusion on DNA. *Phys. Rev. Lett.*, **97**, 1–4.
32. Granéli,A., Yeykal,C.C., Robertson,R.B. and Greene,E.C. (2006) Long-distance lateral diffusion of human Rad51 on double-stranded DNA. *Proc. Natl. Acad. Sci. U.S.A.*, **103**, 1221–1226.
33. Kim,J.H. and Larson,R.G. (2007) Single-molecule analysis of 1D diffusion and transcription elongation of T7 RNA polymerase along individual stretched DNA molecules. *Nucleic Acids Res.*, **35**, 3848–3858.
34. Gorman,J., Chowdhury,A., Surtees,J.A., Shimada,J., Reichman,D.R., Alani,E. and Greene,E.C. (2007) Dynamic basis for one-dimensional DNA scanning by the mismatch repair complex Msh2-Msh6. *Mol. Cell*, **28**, 359–370.
35. Komazin-Meredith,G., Mirchev,R., Golan,D.E., van Oijen,A.M. and Coen,D.M. (2008) Hopping of a processivity factor on DNA revealed by single-molecule assays of diffusion. *Proc. Natl. Acad. Sci. U.S.A.*, **105**, 10721–10726.
36. Laurence,T.A., Kwon,Y., Johnson,A., Hollars,C.W., O'Donnell,M., Camarero,J.A. and Barsky,D. (2008) Motion of a DNA sliding clamp observed by single molecule fluorescence spectroscopy. *J. Biol. Chem.*, **283**, 22895–22906.
37. Gorman,J., Plys,A.J., Visnapuu,M.-L., Alani,E. and Greene,E.C. (2010) Visualizing one-dimensional diffusion of eukaryotic DNA repair factors along a chromatin lattice. *Nat. Struct. Mol. Biol.*, **17**, 932–938.
38. Bonnet,I. and Desbiolles,P. (2011) The diffusion constant of a labeled protein sliding along DNA. *Eur. Phys. J. E. Soft Matter*, **34**, 1–10.
39. Wilkins,D.K., Grimshaw,S.B., Receveur,V., Dobson,C.M., Jones,J.A. and Smith,L.J. (1999) Hydrodynamic radii of native and denatured proteins measured by pulse field gradient NMR techniques. *Biochemistry*, **38**, 16424–16431.
40. Slutsky,M. and Mirny,L.A. (2004) Kinetics of protein-DNA interaction: facilitated target location in sequence-dependent potential. *Biophys. J.*, **87**, 4021–4035.
41. Bagchi,B., Blainey,P.C. and Xie,X.S. (2008) Diffusion constant of a nonspecifically bound protein undergoing curvilinear motion along DNA†. *J. Phys. Chem. B*, **112**, 6282–6284.
42. Schurr,J.M. (1979) The one-dimensional diffusion coefficient of proteins absorbed on DNA. Hydrodynamic considerations. *Biophys. Chem.*, **9**, 413–414.
43. Loverdo,C., Bénichou,O., Voituriez,R., Biebricher,A., Bonnet,I. and Desbiolles,P. (2009) Quantifying hopping and jumping in facilitated diffusion of DNA-binding proteins. *Phys. Rev. Lett.*, **102**, 1–4.